nature climate change

Article

https://doi.org/10.1038/s41558-026-02700-2

Multi-century cooling after net-zero greenhouse gas emissions

Received: 13 March 2025

Accepted: 16 June 2026

Published online: 24 July 2026

Check for updates

Nathaniel Tarshish [1], Nadir Jeevanjee [2] & Inez Fung [3]

Reaching net-zero CO_2 emissions is expected to halt warming, yet whether temperatures remain stable in the centuries after net-zero is poorly constrained. Models exhibit diverse long-term responses to the cessation of CO_2, including additional multi-century warming. Here we analytically predict this post-cessation temperature change, known as the zero emissions commitment (ZEC), from three climate metrics: the airborne fraction of cumulative CO_2 emissions, transient climate response and equilibrium climate sensitivity. Constraining these metrics implies a near-zero multi-century ZEC from historical CO_2 emissions. Net-zero GHG policies, however, differ from idealized CO_2 cessation by targeting the aggregate effect of multiple GHGs and relying on CO_2 removal to offset residual emissions. To capture these policy-relevant effects, we introduce the net-zero emissions commitment (Net-ZEC). Across scenarios and offsetting conventions, Net-ZEC implies a multi-century cooling of at least 0.6 °C following net-zero GHG emissions.

The Paris Agreement aims to strengthen the global response to climate change by limiting warming to well below 2 °C above pre-industrial levels[1]. Limiting warming requires implementing a carbon budget—a cap on total future CO_2 emissions—and reaching net-zero CO_2 emissions before this budget is exhausted.

This paradigm emerged from a series of idealized model experiments that explored the temperature response to CO_2 emissions, ranging from large pulses to sudden cessation[2–5]. These experiments established that CO_2-induced warming is nearly proportional to cumulative emissions[2,3] and that the global temperature remains approximately stable after emissions suddenly cease[4,5]. Any further temperature change after cessation is known as the zero emissions commitment (ZEC)[6]. The proportionality between warming and cumulative emissions underpins the carbon budget and the finding that ZEC ≈ 0 motivates the net-zero CO_2 goal.

To the extent that ZEC deviates from zero, the carbon budget is adjusted to account for this committed temperature change[7,8]. Specifically, the Intergovernmental Panel on Climate Change (IPCC) sets the carbon budget in its Sixth Assessment Report (AR6)[8] using ZEC_{50}, the temperature change 50 years after cessation, which the report assesses at −0.1 °C (5–95% range of −0.3–0.3 °C) based on the climate model ensemble[7] reproduced in Fig. 1. Extending the assessment to multi-century timescales, however, reveals substantially greater divergence and uncertainty. Most of this long-term spread (Fig. 1) remains unexplained, as ZEC is only weakly correlated with standard climate-sensitivity metrics (Extended Data Fig. 1). In light of this longer-term uncertainty, AR6 concludes with very low confidence that the AR6 carbon budgets yield climate stabilization beyond the twenty-first century (Section 5.5.2.3 of ref. 9).

Complicating matters further, ZEC is defined in idealized CO_2-only cessation experiments, yet the policy target of the Paris Agreement is net-zero GHG emissions[1,10]. This distinction is material because non-CO_2 GHGs (methane, nitrous oxide and halogens) together contribute roughly as much warming as CO_2 (ref. 11). Net-zero GHG targets therefore involve offsetting hard-to-abate emissions of these gases with intentional CO_2 removal under a CO_2-equivalence metric, most commonly global warming potential (GWP)[10,12].

After net-zero GHG emissions are reached, AR6 assesses with high confidence that global temperatures stabilize or decline (Section 7.6.2 of ref. 10), citing analyses that primarily address the twenty-first century response[13–16]. On multi-century timescales, however, it is unclear how to reconcile the high confidence in this finding with the

[1]Center for the Environment, Harvard University, Cambridge, MA, USA. [2]Geophysical Fluid Dynamics Laboratory, Princeton, NJ, USA. [3]Department of Earth and Planetary Science, University of California, Berkeley, CA, USA. e-mail: ntarshish@g.harvard.edu

https://doi.org/10.1038/s41558-026-02700-2

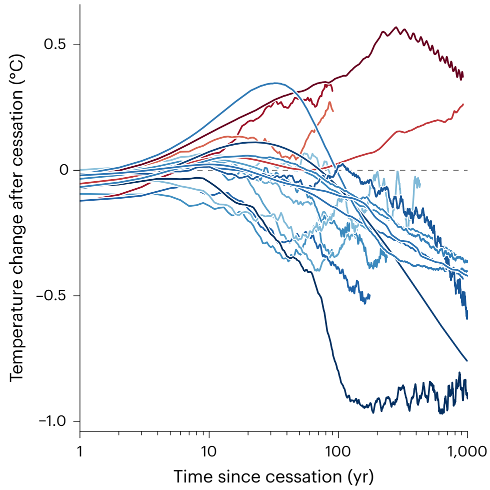

Fig. 1 | Divergent model responses to emissions cessation. Temperature change after emissions cessation in ZECMIP models[7], driven before cessation by a 1% yr^{-1} increase in CO_2 concentration until diagnosed cumulative emissions reach 1,000 GtC. Note the logarithmic *x*-axis scale, which emphasizes inter-model divergence. Figure adapted from ref. 7 under a Creative Commons licence CC BY 4.0.

simultaneously very low confidence that AR6 carbon budgets yield climate stability beyond year 2100[9]. In other words, is the net-zero claim robust to the unexplained long-term ZEC uncertainty shown in Fig. 1?

The following analysis addresses this question. First, long-term ZEC is related to established climate metrics via a simple analytic formula. Constraining these metrics then shows that the substantial additional warming after cessation found in some models in Fig. 1 is inconsistent with other lines of evidence. Second, we clarify the connection between this idealized CO_2-only response and the temperature evolution after net-zero GHG emissions. ZEC is only one component of the full response to net-zero GHGs, which also includes the evolution of non-CO_2 forcing and the continued CO_2 removal necessitated by offsetting. Incorporating these effects yields a robustly negative net-zero emissions commitment (Net-ZEC), defined as the long-term temperature change following the achievement of net-zero GHGs. Net-ZEC therefore bridges the gap between idealized cessation experiments and policy-relevant net-zero pathways.

Climate dynamics after CO_2 cessation

The substantial spread in the post-emissions responses across climate models (Fig. 1) calls for a theoretical explanation. To begin, let CO_2 be the only anthropogenic emission and consider an abrupt cessation of emissions. The equilibrium ZEC[6] is defined as the difference between the equilibrium temperature anomaly T_{eq} and the temperature anomaly at the time CO_2 emissions cease T_{ze},

$$\mathrm{ZEC_{eq}} = T_{\mathrm{eq}} - T_{\mathrm{ze}}. \qquad (1)$$

These anomalies are calculated relative to the pre-industrial baseline. Equilibrium denotes the state reached after multi-century ocean overturning has equilibrated heat and carbon between the atmosphere and ocean, approximated here using model output 1,000 years after emissions cease. This is technically a quasi-equilibrium, as exchange with ocean sediments and silicate weathering over 10–100 kyr will alter ocean alkalinity and return atmospheric CO_2 to pre-industrial levels[17].

This equilibrium temperature can be approximated by rescaling the equilibrium climate sensitivity (ECS), defined as the equilibrium warming given a doubling of CO_2 relative to pre-industrial levels,

$$T_{\mathrm{eq}} = \left(\frac{F_{\mathrm{eq}}}{F_{2\mathrm{x}}}\right) \mathrm{ECS}, \qquad (2)$$

where F_{eq} is the radiative forcing at the equilibrium CO_2 concentration and F_{2x} is the radiative forcing at a doubling of the pre-industrial concentration.

In a similar fashion, the transient temperature at the time of cessation T_{ze} can be found by rescaling the transient climate response (TCR),

$$T_{\mathrm{ze}} = \left(\frac{F_{\mathrm{ze}}}{F_{2\mathrm{x}}}\right) \mathrm{TCR}, \qquad (3)$$

where F_{ze} is the radiative forcing at cessation. By definition, TCR is the temperature anomaly at the time of doubling (year ~70) in the standard 1% yr^{-1} increasing CO_2 experiment. Although measured in this specific scenario, TCR/F_{2x} generally provides an effective conversion from forcing to temperature whenever warming is governed by the fast (5 yr) adjustment of the upper ocean rather than the multi-century deep-ocean mode[18–23]. This scaling closely approximates the global-mean temperature response of GCMs over the historical record; in future projections the neglected deep-ocean mode grows in importance, yet the scaling still captures warming out to 2100 with 10–20% error depending on the scenario[19,20,22,23]. Comparable behaviour is found for the climate emulator used here (Extended Data Fig. 2).

Putting both scalings together gives the approximation,

$$\mathrm{ZEC_{eq}} = \left(\frac{F_{\mathrm{eq}}}{F_{2\mathrm{x}}}\right) \mathrm{ECS} - \left(\frac{F_{\mathrm{ze}}}{F_{2\mathrm{x}}}\right) \mathrm{TCR}. \qquad (4)$$

To simplify further, note that the CO_2 forcing is effectively logarithmic in the CO_2 concentration[24], or equivalently, in the mass of airborne CO_2:

$$F(t) = F_{2\mathrm{x}} \log_2\left(\frac{C_{\mathrm{pre}} + A(t)\, C_{\mathrm{emit}}(t)}{C_{\mathrm{pre}}}\right), \qquad (5)$$

where $A(t)$ is the airborne fraction of cumulative emissions C_{emit} and C_{pre} ≈ 590 GtC is the pre-industrial mass of atmospheric carbon[25]. Substitution into the ZEC formula produces

$$\mathrm{ZEC_{eq}} = \log_2\left(1 + \frac{A_{\mathrm{eq}}\, C_{\mathrm{emit}}}{C_{\mathrm{pre}}}\right) \mathrm{ECS} - \log_2\left(1 + \frac{A_{\mathrm{ze}}\, C_{\mathrm{emit}}}{C_{\mathrm{pre}}}\right) \mathrm{TCR}, \quad (6)$$

where A_{eq} and A_{ze} denote the airborne fractions of cumulative emissions at equilibrium and at the time of emissions cessation, respectively.

Approximating $\log_2(1+x) \propto x$ yields $\mathrm{ZEC_{eq}} \propto (A_{eq}\,\mathrm{ECS} - A_{ze}\,\mathrm{TCR})$. No additional warming after cessation ($\mathrm{ZEC_{eq}} \approx 0$) requires the equality: TCR/ECS ≈ A_{eq}/A_{ze}. The left-hand side measures the disequilibrium in the thermal response of the climate; the right-hand side captures the disequilibrium in the carbon system. Both are mediated by the ocean, yet TCR/ECS depends on radiative physics (Methods) and A_{eq}/A_{ze} reflects the chemistry and biology of CO_2—in the ocean and on land. Therefore, if temperatures are nearly constant after emissions cease, these two quantities are roughly equal despite their disparate origins.

This analysis makes precise prior observations that ZEC simulations are influenced by the degrees of disequilibrium in the carbon system and thermal response[7,26,27] and generalizes the related analytic result of ref. 28 for an idealized carbon-cycle model.

Despite its simplicity, the ZEC formula explains most of the variation across higher-complexity models in ZECMIP (Fig. 2). ZECMIP models were driven with 1% yr^{-1} increase in CO_2 concentration until diagnosed cumulative emissions reached 750 GtC, 1,000 GtC and 2,000 GtC. Figures 1 and 2a correspond to the 1,000 GtC case; see Extended Data Fig. 3 for the 750 GtC and 2,000 GtC cases. The formula is evaluated with the ECS, TCR, F_{2x} and airborne fractions reported in ref. 7, and adapted for the shorter than millennial simulations to predict ZEC at the end of the simulation (Methods). Comparing theory to experiment yields coefficients of determination of $R^2 = 0.74$ for the 1,000 GtC case (Fig. 2a) and $R^2 = 0.79$ when the emissions cases are

https://doi.org/10.1038/s41558-026-02700-2

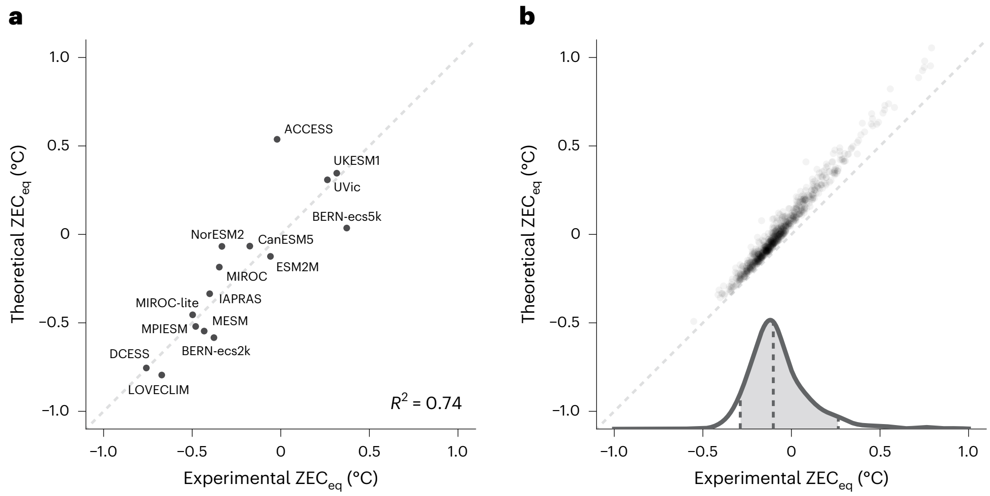

Fig. 2 | Theory captures variation across models of varying complexity. **a**,**b**, Comparison between the analytic formula (equation (6)) and the experimental values for the temperature change after emissions cessation following a 1% yr^{-1} increase in CO_2 up to 1,000 GtC in the ZECMIP ensemble (**a**) and following historical CO_2 emissions in the AR6-tuned FaIR ensemble (**b**). ZECMIP simulations are of varying length and not necessarily in equilibrium (Fig. 1). In **b**, a kernel-density estimate of the FaIR ensemble PDF is also shown with bandwidth set by Silverman's rule[49].

pooled (Extended Data Fig. 3), building confidence that the formula captures the range of responses across the ZECMIP ensemble. Beyond capturing the spread, the formula also pinpoints the sources of inter-model divergence. A Shapley decomposition of equation (6) attributes the ZEC$_{eq}$ of each ZECMIP model to its underlying parameters, showing that uncertainty in carbon and thermal parameters contributes roughly equally to the ensemble spread (Methods; Extended Data Fig. 4).

Constraining with AR6

Linking ZEC to established metrics enables constraining the post-cessation response with several lines of evidence in AR6. This evidence—including process understanding, instrumental warming, palaeoclimate data and emergent constraints[10,29]—informed an ECS estimate of 3.0 [2.0–5.0] °C and a TCR estimate of 1.8 [1.2–2.4] °C (Tables 7.13 and 7.14 of ref. 10). Throughout, bracketed intervals denote the 5–95% range. In 2025, the CO_2 concentration is near 420 ppm, elevated above the pre-industrial value of ~280 ppm by cumulative emissions of $C_{emit} \approx 790$ GtC, yielding an airborne fraction (A_{ze}) near 0.4 (refs. 25,30). Although the equilibrium airborne fraction is not formally assessed in AR6, millennial simulations[7,17] generally find $A_{eq} \approx 0.2$. Inputting these estimates into equation (6) yields ZEC$_{eq} = -0.1$°C—a value close to zero because TCR/ECS $\approx A_{eq}/A_{ze}$ (≈1/2). This finding suggests that the diminishing heat source due to declining atmospheric CO_2 coincidentally balances the declining heat sink from ocean equilibration, yielding minimal temperature change even on multi-century timescales.

To assess the robustness of this estimate, the AR6-calibrated finite amplitude impulse response (FaIR) ensemble is used here to jointly infer TCR, ECS and A_{ze}, accounting for their covariance (Extended Data Fig. 5) and consistent with observations and AR6[31]. FaIR is an energy balance model coupled to an idealized carbon cycle and simple analytic forcing expressions[32–34], used extensively in AR6 for projections and uncertainty assessment[35,36].

Driving the FaIR ensemble with historical CO_2 emissions followed by present-day cessation yields the experimental ZEC$_{eq}$ probability density function (PDF) shown in Fig. 2b. The resulting historical ZEC$_{eq}$ is −0.10 [−0.29 to +0.26] °C, with a 75% probability of cooling, consistent with the sign of most ZECMIP results in Fig. 2a. The median A_{ze} of FaIR is notably lower than that of every ZECMIP model (Extended Data Fig. 6), reflecting the stronger transient carbon sink that emerges when the ensemble is constrained by the historical carbon budget[31]. Although the default ensemble does not sample A_{eq} uncertainty (not assessed in AR6), accounting for the A_{eq} uncertainty implied by ZECMIP broadens the ZEC$_{eq}$ distribution and shifts it more negative: −0.20 [−0.43 to +0.30] °C, with a 78% probability of cooling (Methods; Extended Data Fig. 7). Overall, once constrained by consensus estimates of the key parameters, the ensemble suggests that any additional multi-century warming from past CO_2 emissions is very likely to remain below 0.15 °C (90% probability under both the default and A_{eq}-sampled ensembles).

This small ZEC inferred from the historical case holds broadly across future emissions scenarios. Prescribing CO_2 emissions from the shared socioeconomic pathways (SSPs)[37] through 2100, followed by zero emissions thereafter, yields the FaIR median temperature responses in Fig. 3a. Across SSPs, the median FaIR temperatures remain steady for centuries after cessation, closely mirroring the historical case (black curve in Fig. 3a). See Supplementary Fig. 1 for the full FaIR distributions for each scenario. The weak sensitivity of ZEC$_{eq}$ to cumulative emissions across scenarios is consistent with prior studies[5,26,38,39], which trace this robustness to compensating changes in the carbon and thermal disequilibria.

Incorporating all GHGs

The post-emissions evolution differs substantially when all anthropogenic emissions are considered. At cessation, the total temperature anomaly is decomposed into the contributions from CO_2 and non-CO_2 emissions, respectively: $T_{ze} \approx T_{ze}|_{CO_2} + T_{ze}|_{\text{non-}CO_2}$. After cessation, the non-CO_2 forcing decays on a multidecadal timescale (Extended Data Fig. 8), so that within two centuries CO_2 explains essentially the entire remaining forcing: $F_{eq} \approx F_{eq}|_{CO_2}$ and $T_{eq} \approx T_{eq}|_{CO_2}$.

Accounting for the eventual loss of the non-CO_2 warming in addition to the evolution of CO_2 warming yields a total long-term change after cessation of

$$T_{eq} - T_{ze} \approx \text{ZEC}_{eq} - T_{ze}|_{\text{non-}CO_2}, \tag{7}$$

where ZEC$_{eq} = (T_{eq} - T_{ze})|_{CO_2}$ by definition. Using the fast-mode TCR scaling (equation (3)) to evaluate $-T_{ze}|_{\text{non-}CO_2}$, given AR6 estimates[10] of TCR ≈ 1.8 °C, $F_{2x} = 3.8$ W m^{-2} together with $F_{ze}|_{\text{non-}CO_2} = 0.7$ W m^{-2} in 2025 (ref. 25), yields a cooling of −0.3 °C. This negative contribution is contingent on the heating from non-CO_2 GHGs (+1.7 [1.4–2.0] W m^{-2} in 2025, including ozone exceeding the cooling from aerosols (−1.0 [−1.6 to −0.4] W m^{-2} in 2025)[25].

https://doi.org/10.1038/s41558-026-02700-2

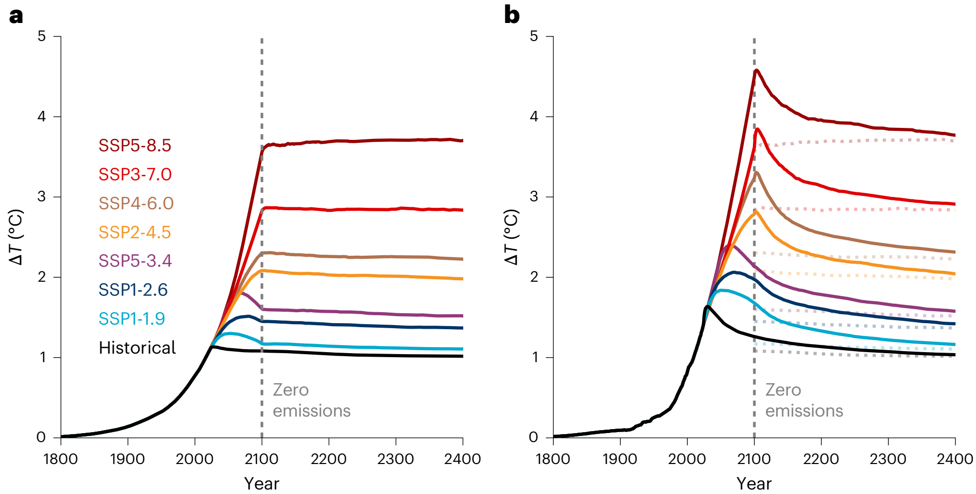

Fig. 3 | Temperature response to emissions cessation. a,**b**, The median temperature response of the FaIR ensemble driven by only CO_2 emissions (**a**) or all emissions (**b**) from the SSPs up to 2100, after which emissions abruptly cease. The historical case (black, with cessation in 2024) is also shown. CO_2-only results are repeated as dashed curves in **b** to facilitate comparison.

Combining this non-CO_2 contribution with the −0.1 °C of cooling from ZEC_{eq} brings the total cessation response to −0.4 °C. In close agreement, FaIR projections find −0.42 [−0.73 to +0.21] °C as shown in Fig. 3b (black curve). Even when $ZEC_{eq} > 0$, cooling in the all-species case still occurs provided that $F_{ze}|_{non\text{-}CO_2} > ZEC_{eq}\,(F_{2x}/\,TCR)$: although 25% of ensemble members exhibit warming under CO_2-only cessation, only 12% yield warming after the cessation of all present-day emissions.

Ceasing emissions in year 2100 after following the SSPs is governed by the same cessation dynamics as the present-day case. As shown in Fig. 3b, the median temperature anomaly (solid curves) relaxes towards the CO_2-only warming (dashed curves) over the ensuing centuries. The resulting long-term change in temperature ranges from −0.57 [−0.89 to −0.31] °C in SSP1-1.9 to −0.97 [−1.82 to +0.81] °C in SSP5-8.5, with 88% to 100% of ensemble members exhibiting cooling depending on the scenario (Supplementary Fig. 2). Because $ZEC_{eq} \approx 0$ holds across scenarios, the magnitude of post-cessation cooling is set by $T_{ze}|_{non-CO_2}$. In year 2100, all SSPs feature larger non-CO_2 forcing than at present, driven by projected declines in sulfate-driven aerosol cooling[40]. However, the magnitude of the non-CO_2 forcing in year 2100 varies by nearly a factor of two across the SSPs, yielding the spread in the inferred commitments (Extended Data Fig. 9). The generality of cooling thus follows from the net non-CO_2 forcing remaining positive across scenarios and throughout this century, as non-CO_2 GHG warming continues to exceed aerosol cooling.

The Net-ZEC

Cooling after emissions cessation has important implications for more policy-relevant pathways, in which emissions do not abruptly cease but rather attain what the Paris Agreement describes as "a balance between anthropogenic emissions by sources and removals by sinks of GHGs in the second half of this century". In practice, achieving this balance often relies on offsetting, in which residual, hard-to-abate non-CO_2 emissions are counterbalanced by net-negative CO_2 emissions. The finite capacity of negative-emissions strategies, however, implies that offsetting cannot be sustained indefinitely and thus requires eventual deep reductions across all major species.

We now examine the temperature commitment in scenarios where net-zero GHG emissions are maintained via offsetting for an extended period before emissions reach negligible levels. The long-term forcing F_{eq}^{offset} reflects the cumulative effect of past offsetting. Contrast this with a cessation experiment, in which emissions cease completely once net-zero GHG emissions is first achieved, yielding a different equilibrium forcing F_{eq}^{cease}. By equation (2), this difference perturbs the equilibrated temperature in the offsetting scenario relative to the cessation case by $ECS\,/F_{2x}\,(F_{eq}^{offset} - F_{eq}^{cease})$.

In the offsetting scenario, we define the eventual change in temperature after net-zero to be the Net-ZEC: -

$$\text{Net-ZEC} = \underbrace{ZEC_{eq} - T_{ze}|_{non\text{-}CO_2}}_{\text{cessation baseline}} + \underbrace{\frac{ECS}{F_{2x}}\left(F_{eq}^{offset} - F_{eq}^{cease}\right)}_{\text{offsetting perturbation}}, \qquad (8)$$

where the cessation baseline is calculated via equation (7) and the perturbation accounts for the additional forcing change accumulated from offsetting.

To evaluate the sign of the offsetting perturbation, recall that the forcing that persists on multi-century timescales is overwhelmingly due to CO_2 (Extended Data Fig. 8). The negative CO_2 emissions required by offsetting reduce this long-term CO_2 forcing relative to the immediate-cessation case:

$$F_{eq}^{offset} < F_{eq}^{cease}. \qquad (9)$$

In this sense, the cessation response provides a general upper bound on the eventual temperature realized in offsetting scenarios.

Quantifying the additional cooling term in equation (8) depends on the details of offsetting, which in turn depend on the metric defining cross-species equivalence. The standard choice in international climate policy is the 100-year GWP (GWP100) which compares the 100-year time-integrated radiative forcing from a pulse emission of a gas to that from an equal-mass pulse of CO_2 (refs. 41,42). Net-zero GHG emissions are therefore defined here as a state in which residual non-CO_2 emissions are balanced by GWP100-equivalent net-negative CO_2 emissions[36]. As shown in Methods, offsetting under GWP100 yields a perturbation forcing that becomes negative within 100 years for all major GHGs. Alternative metric choices are explored in Extended Data Fig. 10 and yield qualitatively similar conclusions (Methods).

To illustrate the cooling that follows net-zero, idealized offsetting pathways are constructed here by modifying the SSP scenarios. Whereas the mitigation SSPs continue past net-zero into sustained net-negative emissions, here net-zero GHG emissions are instead maintained by fixing the emissions composition at the time net-zero

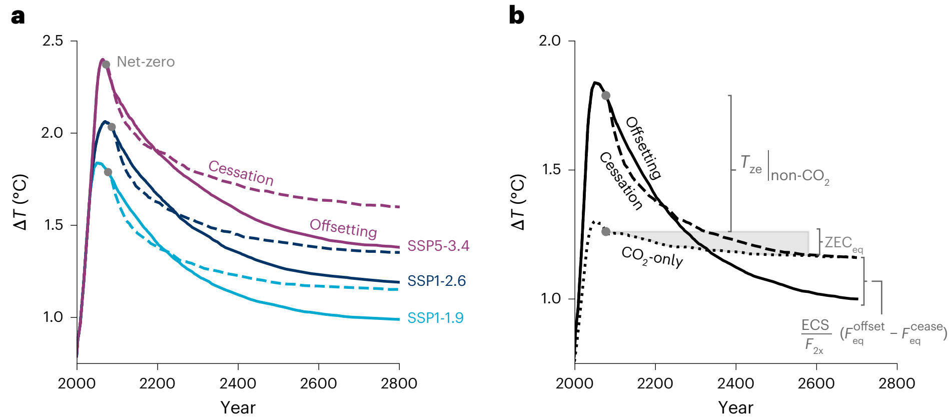

Fig. 4 | Net-zero offsetting yields greater cooling than cessation. a, Median temperature responses of the FaIR ensemble given the mitigation SSPs extended to maintain net-zero exactly via GWP100 offsetting (solid) or cease all emissions at the time of net-zero (dashed). **b**, Decomposition of the net-zero offsetting extension of SSP1-1.9 into the contributions from the disappearance of short-lived warming (solid), the CO_2-only ZEC (dotted) and the perturbation from the cessation baseline (dashed) due to CO_2 removal during GWP offsetting.

is reached and tapering the overall magnitude exponentially on a centennial timescale. These scenarios are not intended to be plausible socioeconomic pathways, but to illustrate the generic cooling predicted by equation (8), which is not expected to depend sensitively on the equivalence metric (Extended Data Fig. 10) or the functional form of tapering.

For these modified variants of the mitigation SSPs, the offsetting (solid) and cessation (dashed) experiments are contrasted in Fig. 4a. As the short-lived non-CO_2 warming fades, the cumulative effect of negative CO_2 emissions becomes apparent, with the net-zero experiment achieving lower multi-century temperatures than the cessation experiment, as anticipated by equations (8) and (9). The Net-ZEC is thus bounded from above by the cessation response, which is comparable across the mitigation SSPs, ranging from −0.60 [−0.90 to −0.25] °C in SSP1-1.9 to −0.73 [−1.14 to −0.18] °C in SSP5-3.4. Independent of the post-net-zero offsetting, the median Net-ZEC is therefore less than −0.6 °C across these scenarios.

The offsetting response can be further understood by decomposing Net-ZEC using equation (8), as illustrated for SSP1-1.9 in Fig. 4b. In this scenario, the median 0.8 °C of cooling arises primarily from the loss of short-lived warming ($-T_{ze}|_{non-CO_2} = -0.5$°C), with smaller contributions from ZEC_{eq} (−0.1 °C) and negative CO_2 emissions during net-zero offsetting (−0.2 °C). With all but four of the 841 ensemble members exhibiting Net-ZEC < 0, this cooling is virtually certain in the AR6-constrained ensemble.

This finding of robust long-term cooling naturally raises questions about the nearer-term trajectory after emissions reach net-zero. Decay of the non-CO_2 forcing drives most of the long-term cooling and substantial decay already occurs within the first few decades (Fig. 4). Recent studies report multidecadal cooling of similar magnitude after cessation[43] and in net-zero stabilization pathways[15,44]. The present study places these findings in a larger context, both theoretically and across time. Near-term cooling is the early expression of a broader multi-century decline, which arises from the short-lived nature of non-CO_2 heating paired with the near-constancy of the CO_2 response and can be estimated from key climate metrics via the simple Net-ZEC formula.

Our evaluation of this formula omits several biogeochemical feedbacks, also commonly absent from climate model projections, including permafrost carbon release[31,45,46]. We provide a preliminary assessment of the impact of these feedbacks on Net-ZEC in Methods; although further study is warranted, available estimates suggest that they are unlikely to overturn the robust Net-ZEC cooling reported here.

Discussion

Linking ZEC_{eq} to established climate metrics (equation (6)) demonstrates that model projections showing substantial post-cessation warming are unlikely when confronted with several lines of evidence. Yet constraining ZEC_{eq} alone is insufficient for characterizing the response to net-zero GHG emissions: the full temperature trajectory emerges from ZEC_{eq} combined with the decay of non-CO_2 forcing and the CO_2 removal required by offsetting. Incorporating these policy-relevant effects yields the Net-ZEC, which provides a relatively comprehensive account of long-term temperature change after net-zero and indicates that sustained net-zero GHG emissions initiate multi-century cooling. Finally, these findings should not be interpreted as implying general climate stability. Regional temperature changes and extremes can deviate from the global mean and continue to evolve after reaching net-zero[47]. Moreover, many climate impacts continue to intensify even under net-zero emissions, including sea-level rise and ocean acidification[5,11,48].

Online content

Any methods, additional references, Nature Portfolio reporting summaries, source data, extended data, supplementary information, acknowledgements, peer review information; details of author contributions and competing interests; and statements of data and code availability are available at https://doi.org/10.1038/s41558-026-02700-2.

References

1. *Paris Agreement Treaty No. XXVII-7-d* (UN, 2015).
2. Allen, M. R. et al. Warming caused by cumulative carbon emissions towards the trillionth tonne. *Nature* **458**, 1163–1166 (2009).
3. Matthews, H. D., Gillett, N. P., Stott, P. A. & Zickfeld, K. The proportionality of global warming to cumulative carbon emissions. *Nature* **459**, 829–832 (2009).
4. Matthews, H. D. & Caldeira, K. Stabilizing climate requires near-zero emissions. *Geophys. Res. Lett.* **35**, 04705 (2008).
5. Solomon, S., Plattner, G.-K., Knutti, R. & Friedlingstein, P. Irreversible climate change due to carbon dioxide emissions. *Proc. Natl Acad. Sci. USA* **106**, 1704–1709 (2009).
6. Hare, B. & Meinshausen, M. How much warming are we committed to and how much can be avoided? *Climatic Change* **75**, 111–149 (2006).
7. MacDougall, A. H. et al. Is there warming in the pipeline? A multi-model analysis of the zero emissions commitment from CO_2. *Biogeosciences* **17**, 2987–3016 (2020).

8. Lee, J. Y. et al. in *Climate Change 2021: The Physical Science Basis* (eds Masson-Delmotte, V. et al.) 553–672 (Cambridge Univ. Press, 2021).
9. Canadell, J. G. et al. in *Climate Change 2021: The Physical Science Basis* (eds Masson-Delmotte, V. et al.) 673–816 (Cambridge Univ. Press, 2021).
10. Forster, P. et al. in *Climate Change 2021: The Physical Science Basis* (eds Masson-Delmotte, V. et al.) 923–1054 (Cambridge Univ. Press, 2021).
11. IPCC: Summary for Policymakers. In: *Climate Change 2021: The Physical Science Basis* (eds Masson-Delmotte, V. et al.) 3–32 (Cambridge Univ. Press, 2021).
12. Lashof, D. A. & Ahuja, D. R. Relative contributions of greenhouse gas emissions to global warming. *Nature* **344**, 529–531 (1990).
13. Bowerman, N. H. S. et al. The role of short-lived climate pollutants in meeting temperature goals. *Nat. Clim. Change* **3**, 1021–1024 (2013).
14. Fuglestvedt, J. S. et al. Implications of possible interpretations of 'greenhouse gas balance' in the Paris Agreement. *Phil. Trans. R. Soc. A* **376**, 20160445 (2018).
15. Tanaka, K. & O'Neill, B. C. The Paris Agreement zero-emissions goal is not always consistent with the 1.5 °C and 2 °C temperature targets. *Nat. Clim. Change* **8**, 319–324 (2018).
16. Schleussner, C.-F. et al. Science and policy characteristics of the Paris Agreement temperature goal. *Nat. Clim. Change* **6**, 827–835 (2016).
17. Archer, D. et al. Atmospheric lifetime of fossil fuel carbon dioxide. *Annu. Rev. Earth Planet. Sci.* **37**, 117–134 (2009).
18. Gregory, J. M. Vertical heat transports in the ocean and their effect on time-dependent climate change. *Clim. Dynam.* **16**, 501–515 (2000).
19. Gregory, J. M. & Forster, P. Transient climate response estimated from radiative forcing and observed temperature change. *J. Geophys. Res. Atmos.* **113**, 23105 (2008).
20. Held, I. M. et al. Probing the fast and slow components of global warming by returning abruptly to preindustrial forcing. *J. Climate* **23**, 2418–2427 (2010).
21. Armour, K. C. Energy budget constraints on climate sensitivity in light of inconstant climate feedbacks. *Nat. Clim. Change* **7**, 331–335 (2017).
22. Jeevanjee, N., Paynter, D. J., Dunne, J. P., Sentman, L. T. & Krasting, J. P. A holistic view of climate sensitivity. *Annu. Rev. Earth Planet. Sci.* **53**, 367–396 (2025).
23. Jeevanjee, N., Paynter, D. J., Dunne, J. P., Sentman, L. T. & Krasting, J. P. On the utility of the transient climate response. *Geophys. Res. Lett.* **53**, e2025GL121354 (2026).
24. Pierrehumbert, R. T. *Principles of Planetary Climate* (Cambridge Univ. Press, 2010).
25. Forster, P. M. et al. Indicators of Global Climate Change 2025: annual update of key indicators of the state of the climate system and human influence. *Earth Syst. Sci. Data* **18**, 3889–3933 (2026).
26. Ehlert, D. & Zickfeld, K. What determines the warming commitment after cessation of CO_2 emissions? *Environ. Res. Lett.* **12**, 015002 (2017).
27. Williams, R. G., Roussenov, V., Frölicher, T. L. & Goodwin, P. Drivers of continued surface warming after cessation of carbon emissions. *Geophys. Res. Lett.* **44**, 10633–10642 (2017).
28. Allen, M. R. et al. Net zero: science, origins, and implications. *Annu. Rev. Environ. Resour.* **47**, 849–887 (2022).
29. Sherwood, S. C. et al. An assessment of Earth's climate sensitivity using multiple lines of evidence. *Rev. Geophy.* **58**, 2019–000678 (2020).
30. Friedlingstein, P. et al. Global carbon budget 2025. *Earth Syst. Sci. Data* **18**, 3211–3288 (2026).
31. Smith, C. et al. fair-calibrate v.1.4.1: calibration, constraining and validation of the FaIR simple climate model for reliable future climate projections. *Geosci. Model Dev.* **17**, 8569–8592 (2024).
32. Smith, C. J. et al. FAIR v.1.3: a simple emissions-based impulse response and carbon cycle model. *Geosci. Model Dev.* **11**, 2273–2297 (2018).
33. Nicholls, Z. R. J. et al. Reduced Complexity Model Intercomparison Project Phase 1: introduction and evaluation of global-mean temperature response. *Geosci. Model Dev.* **13**, 5175–5190 (2020).
34. Leach, N. J. et al. Fair v.2.0.0: a generalized impulse response model for climate uncertainty and future scenario exploration. *Geosci. Model Dev.* **14**, 3007–3036 (2021).
35. IPCC. *Climate Change 2022: Mitigation of Climate Change* (eds Guivarch, C. et al.) 1841–1908 (Cambridge Univ. Press, 2022).
36. Smith, C. et al. in *Climate Change 2021: The Physical Science Basis (Supplementary Material)* (eds Masson-Delmotte, V. et al.) Ch. 7.SM (Cambridge Univ. Press, 2021).
37. Riahi, K. et al. The shared socioeconomic pathways and their energy, land use, and greenhouse gas emissions implications: an overview. *Glob. Environ. Change* **42**, 153–168 (2017).
38. Eby, M. et al. Lifetime of anthropogenic climate change: millennial time scales of potential CO_2 and surface temperature perturbations. *J. Climate* **22**, 2501–2511 (2009).
39. Herrington, T. & Zickfeld, K. Path independence of climate and carbon cycle response over a broad range of cumulative carbon emissions. *Earth Syst. Dynam.* **5**, 409–422 (2014).
40. Meinshausen, M. et al. The shared socio-economic pathway (SSP) greenhouse gas concentrations and their extensions to 2500. *Geosci. Model Dev.* **13**, 3571–3605 (2020).
41. *Decision 24/CP.19: Revision of the UNFCCC reporting guidelines on annual inventories for Parties included in Annex I to the Convention* (UNFCCC, 2014); https://unfccc.int/resource/docs/2013/cop19/eng/10a03.pdf
42. IPCC. *Climate Change 2022: Mitigation of Climate Change* (Cambridge Univ. Press, 2022).
43. Dvorak, M. et al. Estimating the timing of geophysical commitment to 1.5 and 2.0 °C of global warming. *Nat. Clim. Change* **12**, 547–552 (2022).
44. Jenkins, S. et al. The multi-decadal response to net zero CO_2 emissions and implications for emissions policy. *Geophys. Res. Lett.* **49**, e2022GL101047 (2022).
45. Eyring, V. et al. Overview of the Coupled Model Intercomparison Project Phase 6 (CMIP6) experimental design and organization. *Geosci. Model Dev.* **9**, 1937–1958 (2016).
46. Steinert, N. J. & Sanderson, B. M. Normalizing the permafrost carbon feedback contribution to the transient climate response to cumulative carbon emissions and the zero emissions commitment. *Earth Syst. Dynam.* **16**, 1711–1721 (2025).
47. Cassidy, L. J. et al. Regional temperature extremes and vulnerability under net zero CO_2 emissions. *Environ. Res. Lett.* **19**, 014051 (2024).
48. Gillett, N. P., Arora, V. K., Zickfeld, K., Marshall, S. J. & Merryfield, W. J. Ongoing climate change following a complete cessation of carbon dioxide emissions. *Nat. Geosci.* **4**, 83–87 (2011).
49. Silverman, B. W. *Density Estimation for Statistics and Data Analysis* 45 (CRC Press, 1986).

 https://doi.org/10.1038/s41558-026-02700-2

Methods

Fast and slow modes of warming

The two-box model provides a conceptual framework for understanding transient warming in climate models[18,20,21,50]. The lower box represents the deep ocean and the upper box combines the mixed layer of the ocean and the atmosphere. The energy budget of the surface and deep-ocean box, respectively, are approximated as

$$C_s \frac{dT}{dt} = F - \lambda T - \lambda'(T - T_d) - \gamma(T - T_d), \quad (10)$$

$$C_d \frac{dT_d}{dt} = \gamma(T - T_d), \quad (11)$$

where T and T_d are the temperature anomalies (relative to pre-industrial) of the respective boxes; C_s is the heat capacity of the surface ocean (per area with units of J °C^{-1} m^{-2}); F is the radiative forcing (units of W m^{-2}); γ is the heat transfer coefficient between the two ocean layers (units of W m^{-2} °C^{-1}); and λ is the equilibrium feedback parameter, defined as the change in the top-of-atmosphere outgoing radiation per change in surface temperature at equilibrium (in units of W m^{-2} °C^{-1}). Finally, λ' represents the transient deviation in the feedback parameter (also called the pattern effect), driven primarily by cloud and ice-albedo dynamics that evolve with warming (for example, refs. 21,51,52).

When fit to full-complexity simulations, the response of the two-box model can be decomposed into a fast mode that responds to forcing in ~5 years and a slow mode that warms over a few centuries[18,20,53,54]. The fast mode is characterized by a negligible deep-ocean response ($T_d \to 0$) and surface quasi-equilibrium ($C_s\, dT/dt \to 0$):

$$T_{\mathrm{fast}} \approx \frac{F}{\lambda + \lambda' + \gamma}. \quad (12)$$

The magnitude of the fast mode can be calibrated against the standard 1% yr^{-1} increase in CO_2 experiment. In year 70, the forcing corresponds to a CO_2 doubling, $F_{2\times}$ and the temperature anomaly is defined as: $\mathrm{TCR} \approx F_{2\times}/(\lambda + \lambda' + \gamma)$. Substituting this result into equation (12) yields the approximation for the fast-mode response[19,22,23],

$$T_{\mathrm{fast}} \approx \mathrm{TCR}\left(\frac{F}{F_{2\times}}\right), \quad (13)$$

which dominates the temperature response to historical forcing and the SSP forcing extensions out to 2100 (Extended Data Fig. 2).

Alternative offsetting metrics

Although GWP100 is the default metric for aggregating emissions under the United Nations Framework Convention on Climate Change[41], many alternative metrics exist and net-zero GHGs can be defined relative to these as well[10]. Common alternatives include GWP20 and the global temperature-change potential (GTP): by definition, GTP100 compares the temperature anomaly 100 years after a pulse emission of a gas to that from an equal-mass pulse of CO_2 (ref. 55). In the mitigation SSPs, switching metrics from GWP100 to GWP20, GTP50 or GTP100 typically shifts the inferred net-zero date by a few decades (Supplementary Fig. 3).

Applying the same SSP modifications—maintaining net-zero with exponentially declining emissions—under these alternative definitions yields qualitatively similar behaviour (Extended Data Fig. 10). For the SSP1-2.6 modification with CO_2-equivalence defined by GWP20, note that net-zero GHG emissions are approximated by the net emissions in year 2100, which are closer to 1 GtCO_2e than true zero (Supplementary Fig. 3). Relative to the cessation response, GTP generally produces a smaller additional cooling perturbation and the magnitude of a perturbation generally diminishes as the time horizon of the metric increases.

Note that an alternative class of metrics (for example, CGWP, CGTP and GWP*) compares a step change in emissions of short-lived non-CO_2 species to a one-time pulse of CO_2 (refs. 56–58). These metrics arise from an emerging, alternative paradigm that targets net-zero CO_2 alongside approximately stable emissions of non-CO_2 GHGs, rather than net-zero GHGs under a fixed GWP/GTP exchange[10,56–58].

The present analysis supports the view that net-zero CO_2 approximately stabilizes the CO_2 component of warming even on multi-century timescales. For the non-CO_2 warming contribution, the long-term response depends on the emergence of slow-mode warming: even if constant emissions of short-lived species stabilize their forcing, additional warming can still accrue as the slow ocean mode equilibrates. Avoiding continued non-CO_2 warming on multi-century timescales therefore also requires declining non-CO_2 forcing.

Residual forcing from GWP offsetting

Since CO_2 persists in the atmosphere on much longer timescales than any other well-mixed GHG[59], offsetting a pulse of positive non-CO_2 emissions with CO_2 removal of equal GWP100 magnitude ultimately produces a residual net-negative forcing. For the vast majority of species, this net-negative forcing emerges by 100 years, as shown below.

Let $R_X(t)$ denote the radiative forcing response to a unit emission of species X at time $t = 0$. Recall that the absolute GWP over 100 years is $\mathrm{AGWP}100_X = \int_0^{100} R_X(t)\,dt$ and the global warming potential is $\mathrm{GWP}100_X = \mathrm{AGWP}100_X/\mathrm{AGWP}100_{CO_2}$. Under GWP100 neutrality, an emissions pulse of a non-CO_2 species X of magnitude E_X requires a simultaneous emission of $E_{CO_2} < 0$ such that

$$E_X \int_0^{100} R_X(t)\,dt + E_{CO_2} \int_0^{100} R_{CO_2}(t)\,dt = 0. \quad (14)$$

For such a pair, the net perturbation to forcing at $t = 100$ years is

$$\Delta F(100) = R_X(100)\,E_X + R_{CO_2}(100)\,E_{CO_2}. \quad (15)$$

Using equation (14) to eliminate E_{CO_2} and defining the persistence of the forcing as the ratio of the forcing at the end of the 100-year window to its mean over that window $\langle R_X \rangle_{100}$:

$$P_X(100) = \frac{R_X(100)}{\langle R_X \rangle_{100}}, \quad (16)$$

yields the net perturbation forcing in terms of the difference in persistence,

$$\Delta F(100) = \langle R_X \rangle_{100} E_X \left[P_X(100) - P_{CO_2}(100)\right]. \quad (17)$$

The sign of the perturbation is negative if $P_X(100) < P_{CO_2}(100)$, for which a GWP100-neutral exchange of X and CO_2 yields a net-cooling perturbation within 100 years of the emission.

To evaluate this expression, we apply the forcing impulse function for CO_2 in AR6,

$$R_{CO_2}(t) \propto \left[c_0 + c_1 e^{-t/\tau_1} + c_2 e^{-t/\tau_2} + c_3 e^{-t/\tau_3}\right], \quad (18)$$

where $(c_0, c_1, c_2, c_3) = (0.22, 0.22, 0.28, 0.28)$ and $(\tau_1, \tau_2, \tau_3) = (394, 36, 4)$ yr (refs. 60,36). This expression admits an analytic integral, yielding $P_{CO_2}(100) \approx 0.78$.

By comparison, for non-CO_2 GHGs, AR6 approximates the response function as

$$R_X(t) \propto e^{-t/\tau_X}, \quad (19)$$

with τ_X given for each species by the AR6 metrics dataset[36]. In this case, the forcing persistence (with τ_X in years) is

$$P_X(100) = \frac{100\,e^{-100/\tau_X}}{\tau_X\left(1 - e^{-100/\tau_X}\right)}. \quad (20)$$

For the forcing persistence to be greater than the CO_2 value of 0.78, τ_X must be larger than 210 yr according to the above equation.

Most non-CO_2 forcing agents are far shorter-lived than this threshold. The few long-lived F-gases that satisfy $\tau_X > 210$ yr contribute less than 0.02 W m^{-2} to present-day forcing (Supplementary Table 2). Consequently, for the entire remaining non-CO_2 forcing—including methane, N_2O and CFC-12—offsetting under GWP100 yields a net-negative residual forcing within 100 years of emission. This sign reversal in forcing explains why, in Fig. 4b, the offsetting simulation initially exceeds and then crosses below the corresponding cessation experiment roughly a century after net-zero GHGs is first reached.

ZECMIP

Climate model simulations of the CO_2 cessation response following cumulative emissions of 750 GtC, 1,000 GtC and 2,000 GtC are sourced from experiments A1–A3 in ref. 7. In particular, the cessation temperature T_{ze} is taken from the values reported by each modelling group, computed as a centred 20-year average in the parent 1% yr^{-1} CO_2 experiment. Many ZECMIP simulations are of too-short duration to capture the full carbon and thermal equilibria. The equilibrium ZEC formula is modified here to describe the final state realized by each simulation. The final temperature T_f is first measured by averaging over the last 20 years of the simulation. If the simulation is out of thermal equilibrium, planetary energy balance gives $\epsilon N_f = F_f - \lambda T_f$, where N_f is the top-of-atmosphere energy imbalance (W m^{-2}) and ϵ is the efficacy of planetary heat uptake[20,61]. Replacing T_{eq} with $T_f = (F_f - \epsilon N_f)/\lambda$ in equation (4) gives:

$$\mathrm{ZEC_f} = \left(\frac{F_f - \epsilon N_f}{F_{2x}}\right)\ \mathrm{ECS} - \left(\frac{F_{ze}}{F_{2x}}\right)\ \mathrm{TCR}, \qquad (21)$$

which enables application of the ZEC formula to the full ZECMIP dataset, with results shown in Fig. 2a. The forcings are evaluated from $F(t) = F_{2x}\log_2(\mathrm{CO_2}(t)/\mathrm{CO_{2,pre}})$ given the F_{2x} values reported in ref. 7. Note that some models have non-zero initial N due to energy-conservation error or insufficient spin-up. We compute N_f relative to this pre-industrial imbalance, estimated as the y-intercept of a linear regression of N versus F over the first 20 years (Supplementary Fig. 4). The efficacy ϵ of each model is treated as constant and values are taken from ref. 7, who fit ϵ to years 10–140 of the 1% yr^{-1} CO_2 simulation.

Several models appear in Fig. 1 but not in Fig. 2 because of data availability constraints. In ZECMIP, N is not reported for BERN-ecs3k, CLIMBER2 and CNRM-ESM2-1; ϵ and F_{2x} for CESM are also not available[7]. Finally, PLASIM-GENIE is excluded as implausible on the grounds that its equilibrated warming (T_{eq}) decreases with increasing cumulative emissions.

FaIR

To understand how estimates of key climate metrics covary and to project future temperatures in line with AR6 uncertainties, we rely on a reduced-complexity model ensemble. Reduced-complexity models can be run in larger ensembles and more effectively tuned to match target distributions than resource-intensive CMIP models[33]. Here we use the FaIR ensemble, arising from IPCC efforts to build a model ensemble consistent with their integrated assessments[31,32,34,62]. We rely on the AR6-tuned FaIR ensemble, which is fully described in ref. 34 and calibrated to AR6 in ref. 31.

We briefly note that FaIR consists of a three-layer energy balance coupled to a basic carbon-cycle model. Carbon uptake is parameterized via a four-timescale impulse response function with state-dependent adjustments to incorporate carbon–climate feedbacks. Simple treatments of methane chemistry, aerosol direct and cloud-interaction effects and other minor GHGs are also included (see ref. 34 for details) and calibrated to match AR6 distributions[31]. For the historical ZEC experiment, we drive the FaIR ensemble with the latest indicators of global climate change (IGCC) emissions reconstruction[25]. Note that the land-use albedo forcing is excluded from this analysis, as in standard ZEC setups[43,63], although FaIR sensitivity tests have shown that including it has little impact[43]. Future projections are driven with emissions from the SSPs[40]. In ZEC experiments, anthropogenic emissions are zeroed by instantaneously reverting all emissions to pre-industrial (1750) baselines and T_{ze} is evaluated at the timestep immediately before this cessation and therefore does not include any of the subsequent aerosol decay.

The default FaIR calibration fixes A_{eq} at 0.22—the multimodel mean following pulse emissions in ref. 60—and does not sample its uncertainty, which has not been formally assessed in AR6. To probe the sensitivity of our results to A_{eq}, we recompute the FaIR equilibrium temperature with A_{eq} Monte Carlo sampled from a statistical distribution informed by the millennial-scale ZECMIP results. Across these millennial-scale runs, A_{eq} varies remarkably linearly with cumulative emissions across the 750 GtC, 1,000 GtC and 2,000 GtC pulses (Extended Data Fig. 7a). The linear $A_{eq}(C_{emit})$ relationship for each model is interpolated to FaIR historical cumulative emissions ($C_{emit} \approx 740$ GtC; refs. 25,30), yielding one A_{eq} per ZECMIP model. The resulting A_{eq} uncertainty range for historical emissions spans 0.16–0.27 with a median of 0.18. The Monte Carlo ensemble computes the equilibrium temperatures from every such A_{eq} paired with every FaIR configuration. Sampling across this range shifts the ZEC$_{eq}$ distribution towards more negative values, ZEC$_{eq}$ = − 0.20 [−0.43 to +0.30] °C and yields a 78% probability of cooling (Extended Data Fig. 7). Put differently, at FaIR median parameters, A_{eq} would need to reach ~0.23 to flip ZEC$_{eq}$ positive—a value exceeded only by UVic ($A_{eq} = 0.27$), with IAPRAS ($A_{eq} = 0.23$) sitting exactly at the sign-change boundary (Extended Data Fig. 7). Thus, even after accounting for A_{eq} uncertainty, ZEC$_{eq}$ likely remains small in magnitude and weakly negative.

Sources of intermodel spread

We now evaluate sources of intermodel spread in ZEC$_{eq}$ across the ZECMIP ensemble, using the FaIR ensemble median as a baseline. To facilitate this, we perform the ZECMIP-A1 experiment (a 1% yr^{-1} concentration-driven ramp until diagnosed emissions reach 1,000 GtC) with the FaIR ensemble (Supplementary Fig. 5). Under this protocol, FaIR yields ZEC$_{eq}$ = −0.16 [−0.48 to +0.43] °C, slightly more negative and substantially more uncertain than the historical-cessation value of −0.10 [−0.29 to +0.26] °C. The narrower historical range reflects the observational constraints on temperature and CO_2 to which FaIR has been calibrated. The offset in median ZEC$_{eq}$ follows from the rapid 1% yr^{-1} ramp leaving a higher airborne fraction at cessation ($A_{ze} = 0.48$ in A1 versus 0.41 historical).

We now investigate the root causes of spread within the ZECMIP ensemble. For model m, let $\mathrm{ZEC}_{eq}^{th,m}$ denote the equilibrium ZEC formula (equation (6)) evaluated at $C_{emit} = 1{,}000$ GtC and the parameters of the model (ECS, TCR, A_{ze}, A_{eq}) and let the residual between this theoretical estimate and the experimental value $\mathrm{ZEC}_{eq}^{exp,m}$ be denoted ε_m. The difference between a given ZECMIP model and FaIR ensemble median is then

$$\mathrm{ZEC}_{eq}^{exp,m} - \mathrm{ZEC}_{eq}^{exp,\,FaIR} = \left(\mathrm{ZEC}_{eq}^{th,m} - \mathrm{ZEC}_{eq}^{th,FaIR}\right) + (\varepsilon_m - \varepsilon_{FaIR}), \qquad (22)$$

where $\mathrm{ZEC}_{eq}^{exp,\,FaIR}$ represents the median FaIR experimental value and $\mathrm{ZEC}_{eq}^{th,FaIR}$ the theoretical prediction given the median of FaIR parameter values. The residual for FaIR is $\varepsilon_{FaIR} = 0.03$ °C.

Consider attributing the difference in theoretical estimates $\mathrm{ZEC}_{eq}^{th,m} - \mathrm{ZEC}_{eq}^{th,FaIR}$ to the underlying parameters (ECS, TCR, A_{ze}, A_{eq}) by exchanging the FaIR parameter values one-by-one for those of model m and re-evaluating the formula. The ordering of this sequence of exchanges impacts the attribution because the ZEC formula is nonlinear. The Shapley value[64] resolves this by averaging the effect of the exchange of parameter over all possible orderings of the exchanges (4! = 24 cases), yielding unambiguous per-parameter attributions that sum exactly to the theoretical difference (Extended Data Fig. 4).

This Shapley decomposition reveals two recurring patterns. First, every ZECMIP-A1 model carries a higher A_{ze} than the FaIR median (Extended Data Fig. 6), systematically driving the ZEC_{eq} of each model more negative. The transient carbon sink of FaIR, calibrated to the historical carbon budget, is apparently stronger than that of any ZECMIP model. Second, contributions from ECS and TCR largely cancel across the ensemble because the two parameters covary: models with low ECS also tend to have low TCR. The exceptions are BERN-ecs5k, whose prescribed ECS = 5.3 °C is only partly compensated by its elevated TCR and UVic, whose ECS = 3.7 °C also outstrips its near-median TCR. Additional warming in UVic is driven by an unusually high A_{eq} = 0.29 for the 1,000 GtC case (compared with an ensemble mean of 0.21). Across the ensemble, variations in both the thermal and carbon response interplay to drive spread (Extended Data Fig. 4).

Neglected biogeochemical feedbacks

FaIR does not include several 'biogeochemical feedbacks' (listed in Supplementary Table 1), which are expected to modify the radiative forcing. The biogeochemical processes not resolved in this simple climate model (and missing from the majority of ESMs and CMIP6 projections[45]) are assessed by the IPCC[9] to include positive feedbacks—such as the permafrost CO_2 response (+0.09 ±0.06 W m^{-2} °C^{-1}), the permafrost CH_4 response (+0.01 ± 0.011 W m^{-2} °C^{-1}) and increases in wetland CH_4 sources (+0.03 ± 0.01 W m^{-2} °C^{-1})—along with negative feedbacks, including the increase in natural BVOC sources with warming (−0.05 ± 0.10 W m^{-2} °C^{-1}) and the sea-salt response to climate (−0.05 ± 0.05 W m^{-2} °C^{-1}). Taken together, these neglected processes (listed in Supplementary Table 1) sum to a neglected biogeochemical feedback factor of α = 0.04 ± 0.14 W m^{-2} °C^{-1}.

Accounting for these additional feedbacks would therefore be expected to increase the equilibrated radiative forcing by an amount $\Delta F_{eq} = \alpha T_{eq}$, elevating the final temperature by approximately $\Delta T_{eq} \approx \alpha T_{eq}/\lambda$ (via equation (2)). The fractional change in T_{eq} is thus $\alpha/\lambda \approx 0.03$ (± 0.11) and including these additional feedbacks increases the equilibrated temperature anomalies by several percentage points. Reversing the long-term cooling found in Fig. 4b, however, requires a much larger correction of near 70%.

The permafrost carbon feedback, however, warrants further attention because, unlike the other neglected processes, the release of CO_2 from thawing permafrost is cumulative and thaw is expected to persist on multi-century timescales[9,65]. As a rough benchmark, offsetting the 0.8 °C NZEC cooling with permafrost warming would require on the order of 500 GtC of additional cumulative CO_2 emissions from permafrost (using the AR6 best-estimate TCRE of 1.65 °C per 1,000 GtC). This mass is comparable to the entire organic carbon stock in the upper metre of permafrost regions[66]. The AR6 assessment of permafrost carbon release is an order of magnitude smaller (18 [3–41] GtC per °C of global warming) but covers thaw only out to 2100 (Box 5.1 of ref. 9). AR6 expresses low confidence in the timing and magnitude of release beyond that horizon, as modelling permafrost on multi-century timescales is an open challenge[9]. Permafrost modules are not implemented in most CMIP models and the land models that do include permafrost yield widely differing projections for permafrost soil carbon[67].

The available evidence, although limited, suggests that multi-century thaw falls short of mobilizing the entire upper metre of permafrost[68,69]. In particular, ref. 68 reported cumulative permafrost release of 178 [70–346] GtC over 500 years following CO_2 cessation in UVic[70], yielding +0.27 [0.12–0.49] °C of permafrost-induced warming. We view this as an upper bound: UVic exhibits ZEC > 0 even without permafrost feedbacks (Fig. 3a of ref. 68), so this estimate combines a lagged thaw response to prior warming with intensifying thaw driven by continued post-cessation warming. Our NZEC scenarios, by contrast, exhibit temperature decline after emissions reach net-zero GHGs. Our scenarios are thus closer to the temperature-stabilization protocol of ref. 69, which isolates the emissions due to the lagged component of thaw using the same UVic permafrost module[70]. In these simulations, temperature is prescribed to stabilize at 2 °C in year 2060, following historical emissions extended by SSP2-4.5. An additional ~50 [22–75] GtC of permafrost carbon is then released between stabilization and the end of the simulation in 2300. Release decelerates strongly after stabilization: ~20 [15–25] GtC is emitted between stabilization in 2060 and 2100, compared with ~4 [0–7] GtC over the final 40 years (2260–2300) of the simulation (Fig. 3c of ref. 69). Linearly extrapolating this end-of-simulation rate to a full millennium past stabilization for each ensemble member yields a cumulative post-stabilization release of ~116 [22–206] GtC. Because thaw decelerates over the simulated period, this linear extrapolation is likely an overestimate. Applying the AR6 TCRE scaling to this millennial-scale release suggests an additional 0.19 [0.04–0.34] °C of warming from permafrost. Although rudimentary, this extrapolation suggests that permafrost is unlikely to reverse the NZEC cooling reported here. Further research is clearly warranted, however, given the sparsity of permafrost-enabled millennial-scale simulations and models, along with the omission of abrupt thaw and wildfire-driven carbon loss[71].

Finally, we note that a further high-latitude process not fully captured by FaIR may act in the opposite direction: the northward expansion of boreal forests. Most of the C4MIP models used to tune the carbon cycle of FaIR lack dynamic vegetation, yet there is evidence that such effects could drive high-latitude carbon uptake at magnitudes comparable to permafrost loss[72].

Data availability

The datasets analysed in this study are publicly available from their original sources: the ZECMIP model output from ref. 7; the AR6-calibrated FaIR ensemble and forcing data from refs. 31,34; the historical emissions reconstruction from the Indicators of Global Climate Change dataset[25]; and the SSP emissions from ref. 40. The processed data generated in this study are available via Zenodo at https://doi.org/10.5281/zenodo.10120439 (ref. 73).

Code availability

The code used to perform the analysis and generate the figures in this study are available via Zenodo at https://doi.org/10.5281/zenodo.10120439 (ref. 73).

References

50. Jeevanjee, N. Climate sensitivity from radiative-convective equilibrium: a chalkboard approach. *Am. J. Phys.* **91**, 731–745 (2023).
51. Rose, B. E., Armour, K. C., Battisti, D. S., Feldl, N. & Koll, D. D. The dependence of transient climate sensitivity and radiative feedbacks on the spatial pattern of ocean heat uptake. *Geophys. Res. Lett.* **41**, 1071–1078 (2014).
52. Andrews, T. et al. On the effect of historical SST patterns on radiative feedback. *J. Geophys. Res. Atmos.* **127**, e2022JD036675 (2022).
53. Olivié, D. J. L., Peters, G. P. & Saint-Martin, D. Atmosphere response time scales estimated from AOGCM experiments. *J. Climate* **25**, 7956–7972 (2012).
54. Geoffroy, O. et al. Transient climate response in a two-layer energy-balance model. Part i: Analytical solution and parameter calibration using CMIP5 AOGCM experiments. *J. Climate* **26**, 1841–1857 (2013).
55. Shine, K. P., Fuglestvedt, J. S., Hailemariam, K. & Stuber, N. Alternatives to the global warming potential for comparing climate impacts of emissions of greenhouse gases. *Climatic Change* **68**, 281–302 (2005).

56. Cain, M. et al. Improved calculation of warming-equivalent emissions for short-lived climate pollutants. *npj Clim. Atmos. Sci.* **2**, 29 (2019).
57. Lynch, J., Cain, M., Pierrehumbert, R. & Allen, M. Demonstrating GWP*: a means of reporting warming-equivalent emissions that captures the contrasting impacts of short- and long-lived climate pollutants. *Environ. Res. Lett.* **15**, 044023 (2020).
58. Collins, W. J., Frame, D. J., Fuglestvedt, J. S. & Shine, K. P. Stable climate metrics for emissions of short and long-lived species—combining steps and pulses. *Environ. Res. Lett.* **15**, 024018 (2020).
59. Dentener, F.J. et al. *Climate Change 2021: The Physical Science Basis* (eds Masson-Delmotte, V. et al.) 2139–2152 (Cambridge Univ. Press, 2021).
60. Joos, F. et al. Carbon dioxide and climate impulse response functions for the computation of greenhouse gas metrics: a multi-model analysis. *Atmos. Chem. Physics* **13**, 2793–2825 (2013).
61. Winton, M., Takahashi, K. & Held, I. M. Importance of ocean heat uptake efficacy to transient climate change. *J. Climate* **23**, 2333–2344 (2010).
62. Millar, R. J., Nicholls, Z. R., Friedlingstein, P. & Allen, M. R. A modified impulse-response representation of the global near-surface air temperature and atmospheric concentration response to carbon dioxide emissions. *Atmos. Chem. Physics* **17**, 7213–7228 (2017).
63. Jones, C. D. et al. The zero emissions commitment model intercomparison project (ZECMIP) contribution to C4MIP: quantifying committed climate changes following zero carbon emissions. *Geosci. Model Dev.* **12**, 4375–4385 (2019).
64. Shapley, L.S. in *Contributions to the Theory of Games*. Vol. II. *Annals of Mathematics Studies* (eds Kuhn, H.W. & Tucker, A.W.) 307–317 (Princeton Univ. Press, 1953).
65. Schuur, E. A. G. et al. Expert assessment of vulnerability of permafrost carbon to climate change. *Climatic Change* **119**, 359–374 (2013).
66. Hugelius, G. et al. Estimated stocks of circumpolar permafrost carbon with quantified uncertainty ranges and identified data gaps. *Biogeosciences* **11**, 6573–6593 (2014).
67. McGuire, A. D. et al. Dependence of the evolution of carbon dynamics in the northern permafrost region on the trajectory of climate change. *Proc. Natl Acad. Sci. USA* **115**, 3882–3887 (2018).
68. MacDougall, A. H. Estimated effect of the permafrost carbon feedback on the zero emissions commitment to climate change. *Biogeosciences* **18**, 4937–4952 (2021).
69. Cui, M., Ji, D. & Chen, Y. Permafrost response and feedback under temperature stabilization and overshoot scenarios with different global warming levels. *Earth Syst. Dynam.* **16**, 1809–1831 (2025).
70. MacDougall, A. H. & Knutti, R. Projecting the release of carbon from permafrost soils using a perturbed parameter ensemble modelling approach. *Biogeosciences* **13**, 2123–2136 (2016).
71. Schädel, C. et al. Permafrost and wildfire carbon emissions indicate need for additional action to keep Paris Agreement temperature goals within reach. *Commun. Earth Environ.* **7**, 306 (2026).
72. Pugh, T. A. M. et al. A large committed long-term sink of carbon due to vegetation dynamics. *Earth's Future* **6**, 1413–1432 (2018).
73. Tarshish, N. Repository for "Multi-century cooling after net-zero greenhouse gas emissions". *Zenodo* https://doi.org/10.5281/zenodo.10120439 (2026).

Acknowledgements

N.T. acknowledges the support of the Harvard University Center for the Environment.

Author contributions

N.T. and N.J. designed the research. N.T. derived the formalism, performed the analysis and wrote the paper. N.T., N.J. and I.F. revised the paper.

Funding

N.T. was supported by the Kernan Brothers Environmental Fellowship at the Harvard University Center for the Environment.

Competing interests

The authors declare no competing interests.

Additional information

Extended data is available for this paper at https://doi.org/10.1038/s41558-026-02700-2.

Supplementary information The online version contains supplementary material available at https://doi.org/10.1038/s41558-026-02700-2.

Correspondence and requests for materials should be addressed to Nathaniel Tarshish.

Peer review information *Nature Climate Change* thanks Chris Jones and the other, anonymous, reviewer(s) for their contribution to the peer review of this work.

https://doi.org/10.1038/s41558-026-02700-2

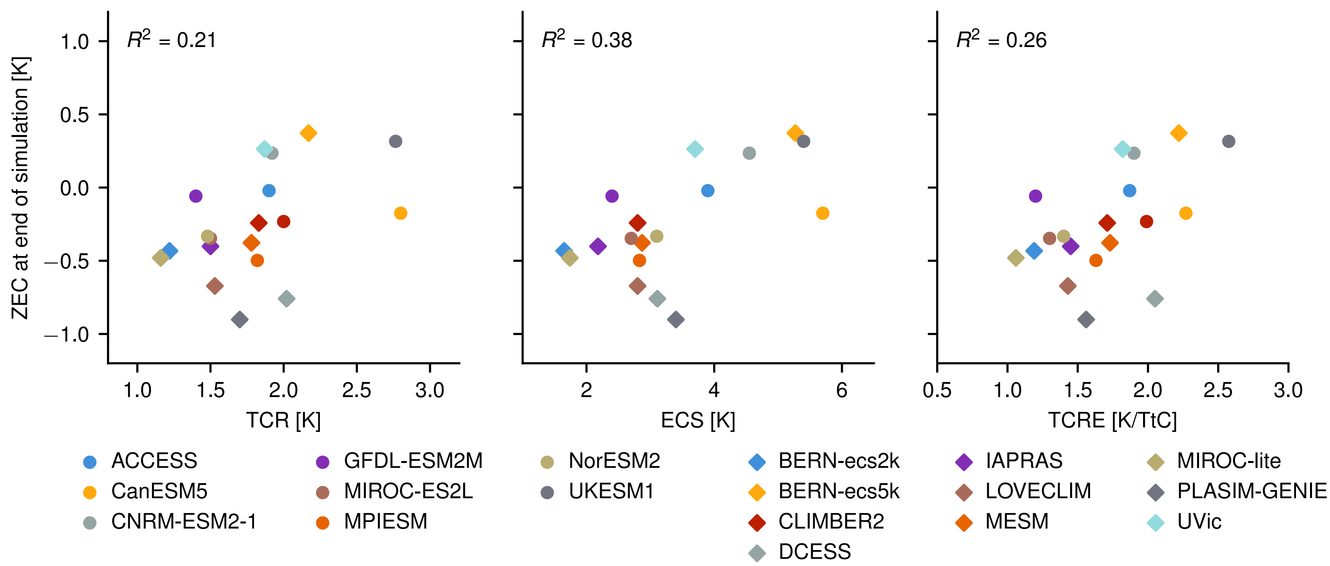

Extended Data Fig. 1 | ZEC correlates weakly with established metrics. Correlations between ZEC realized in the ZECMIP 1000 GtC simulations (of varying duration) shown in Fig. 1 of the main text and the transient climate response (left), equilibrium climate sensitivity (center), and the transient climate response to cumulative emissions (right). Climate metrics are sourced from ZECMIP documentation[7].

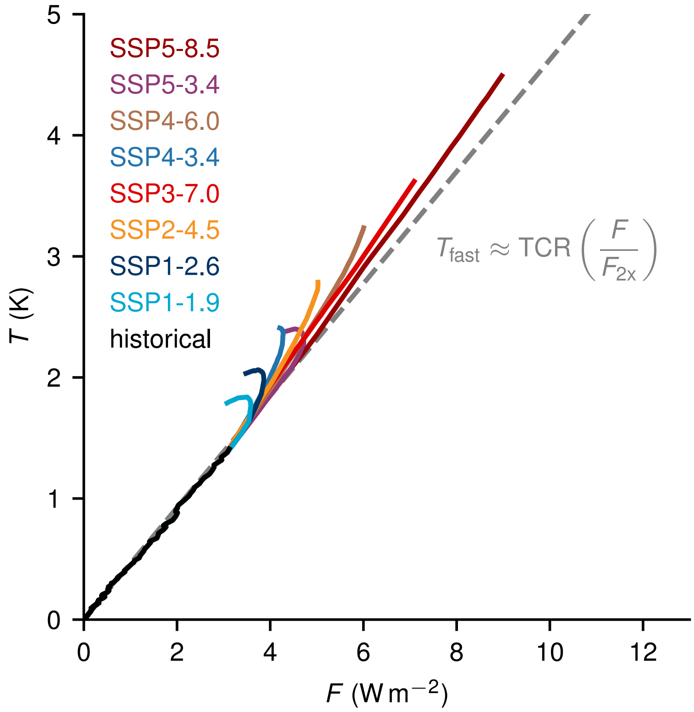

Extended Data Fig. 2 | Fast-mode response dominates historical and near-term temperature rise. Median FaIR ensemble globalmean temperature change versus total radiative forcing for the historical period (black) and SSP extensions (colors). Mitigation SSPs are shown until they reach net-zero GHG emissions; other SSPs are shown through 2100. The dashed line shows the fast-mode prediction. By late century the slow mode becomes apparent, contributing roughly 10–20% of total warming depending on the scenario.

https://doi.org/10.1038/s41558-026-02700-2

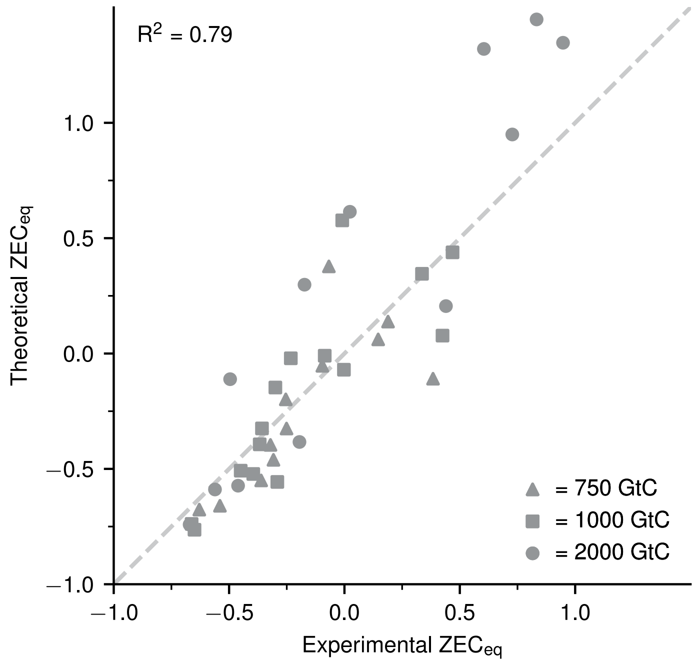

Extended Data Fig. 3 | Theory compared to all ZECMIP experiments. Comparison between the analytic formula (Eq. 6) and the experimental values for the temperature change after emissions cessation following a 1%/yr increase in CO2 up to 750 (triangles), 1000 GtC (squares), and 2000 GtC (circles) in the ZECMIP ensemble.

https://doi.org/10.1038/s41558-026-02700-2

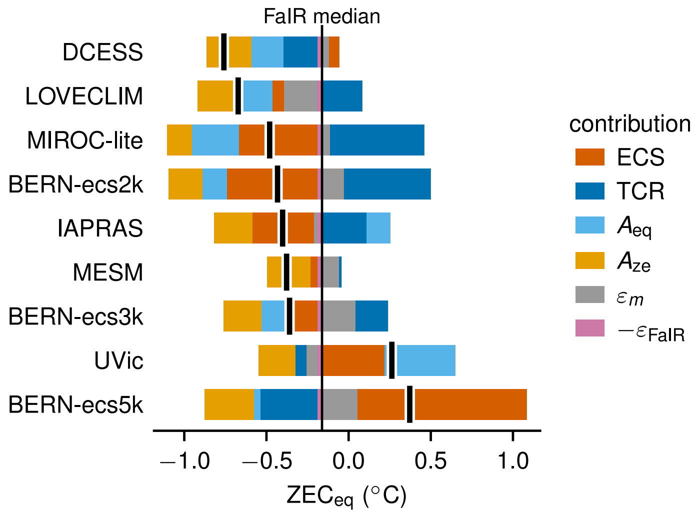

Extended Data Fig. 4 | Shapley decomposition of ZECMIP-FaIR differences. Each row corresponds to a ZECMIP-A1 long-running model. Within a row, horizontal bars stack the per-parameter Shapley contributions for (ECS, TCR, A_{eq}, A_{ze}) along with the off-theory residual difference ε_m - ε_{FaIR}, accumulating outward from the FaIR median ZEC$_{eq}$ (vertical line) to the model's reported ZEC$_{eq}$ (black tick). Rightward segments indicate parameters that push a model toward additional post-cessation warming (high ECS or A_{eq}, or low TCR or A_{ze}); leftward segments indicate the opposite tendencies, driving post-cessation cooling.

https://doi.org/10.1038/s41558-026-02700-2

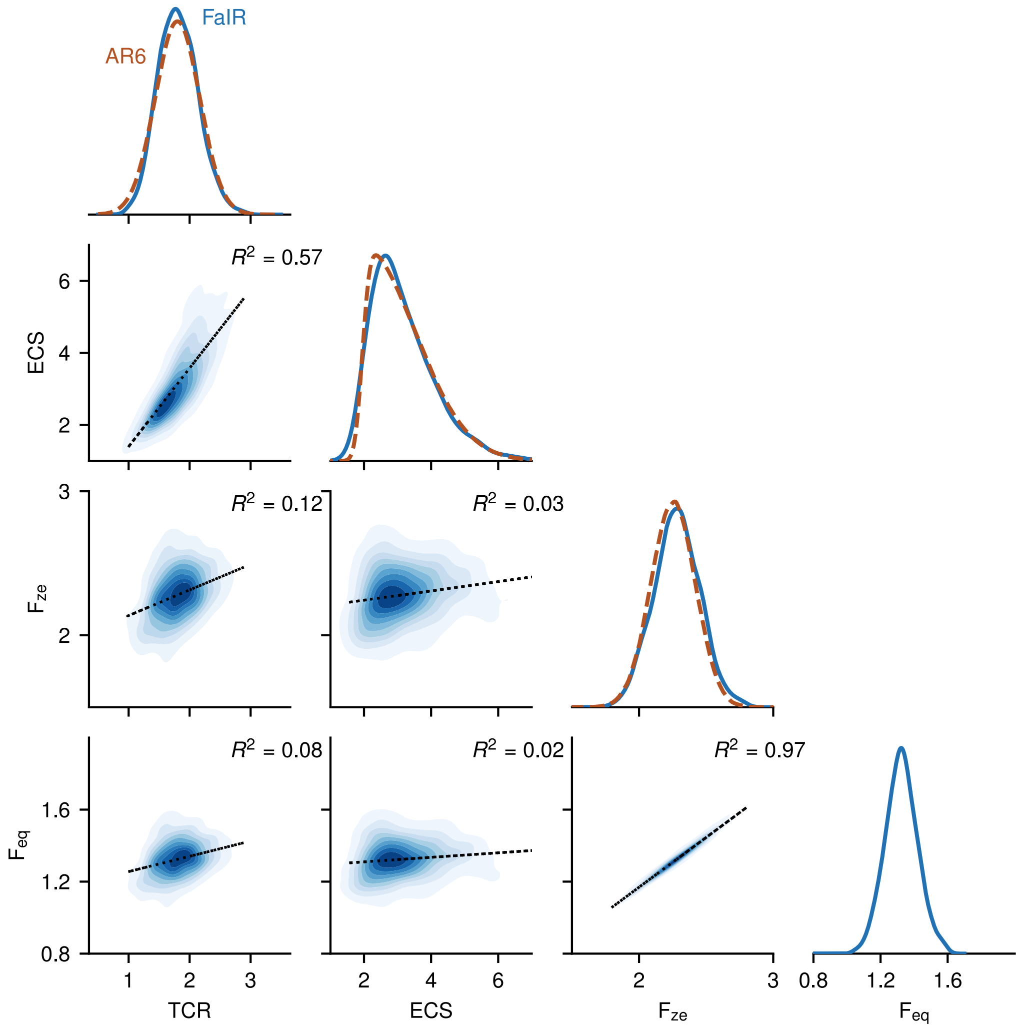

Extended Data Fig. 5 | Estimates of distributions and covariances in the AR6-tuned FaIR ensemble. Diagonals present the kernel density estimates of the 841-member ensemble of FaIR configurations, tuned to the AR6 report. See Methods for details. Off-diagonals show the kernel-density estimates for covariances between the different variables that determine ZEC. The ensemble's TCR and ECS distribution are compared to the AR6 estimates. The present-day CO_2 forcing, in this context, F_{ze}, is compared to the best estimate of 2023 forcing based on AR6 methods[25]. The forcing at carbon equilibrium is not assessed in AR6, so no comparison is made.

https://doi.org/10.1038/s41558-026-02700-2

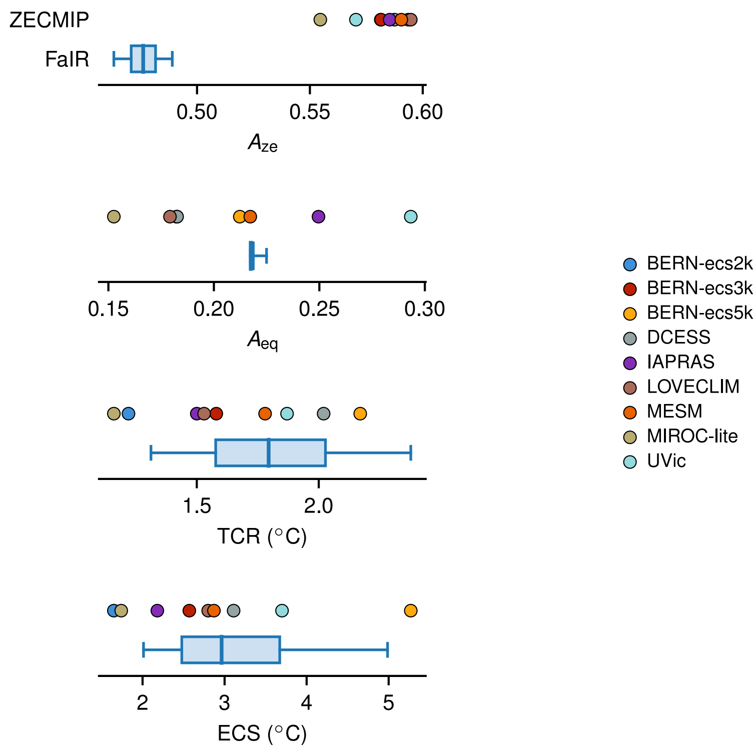

Extended Data Fig. 6 | Comparing FaIR and ZECMIP parameters. Per-parameter distributions under the ZECMIP-A1 protocol: the FaIR 841-config ensemble is shown as a horizontal box-and-whisker (box: 25–75%; whiskers: 5–95%; line: median), with each ZECMIP-A1 long-running model overlaid as a colored point.

https://doi.org/10.1038/s41558-026-02700-2

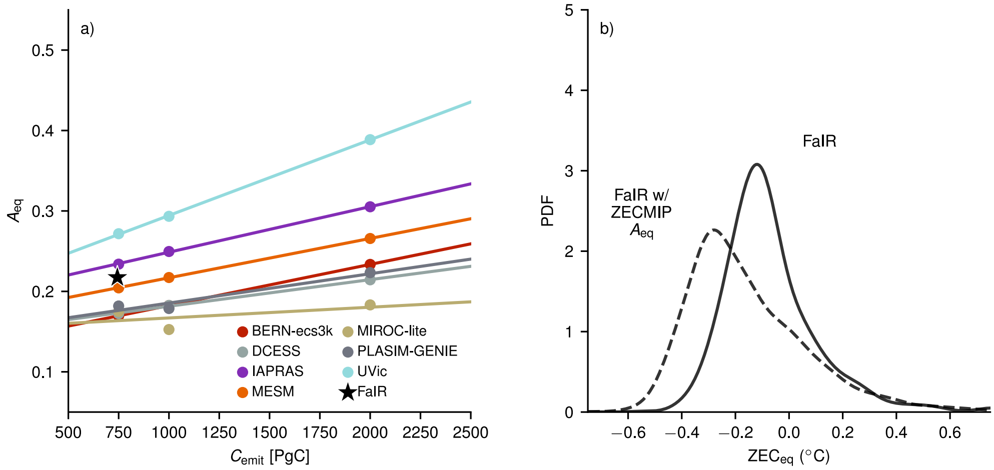

Extended Data Fig. 7 | ZECMIP-sampled equilibrium airborne fraction shifts ZEC_eq more negative. (**a**) Aeq as a function of cumulative emissions for the millennial-scale ZECMIP models (colored points: 750, 1000, and 2000 GtC pulses; lines: linear fits used to interpolate to other emissions). The black star marks FaIR's default A_{eq} at the ensemble-median cumulative emissions. (**b**) FaIR's ZEC_{eq} distribution under the historical cessation experiment with the default A_{eq} (solid) and with A_{eq} Monte Carlo sampled from the ZECMIP fits (dashed).

https://doi.org/10.1038/s41558-026-02700-2

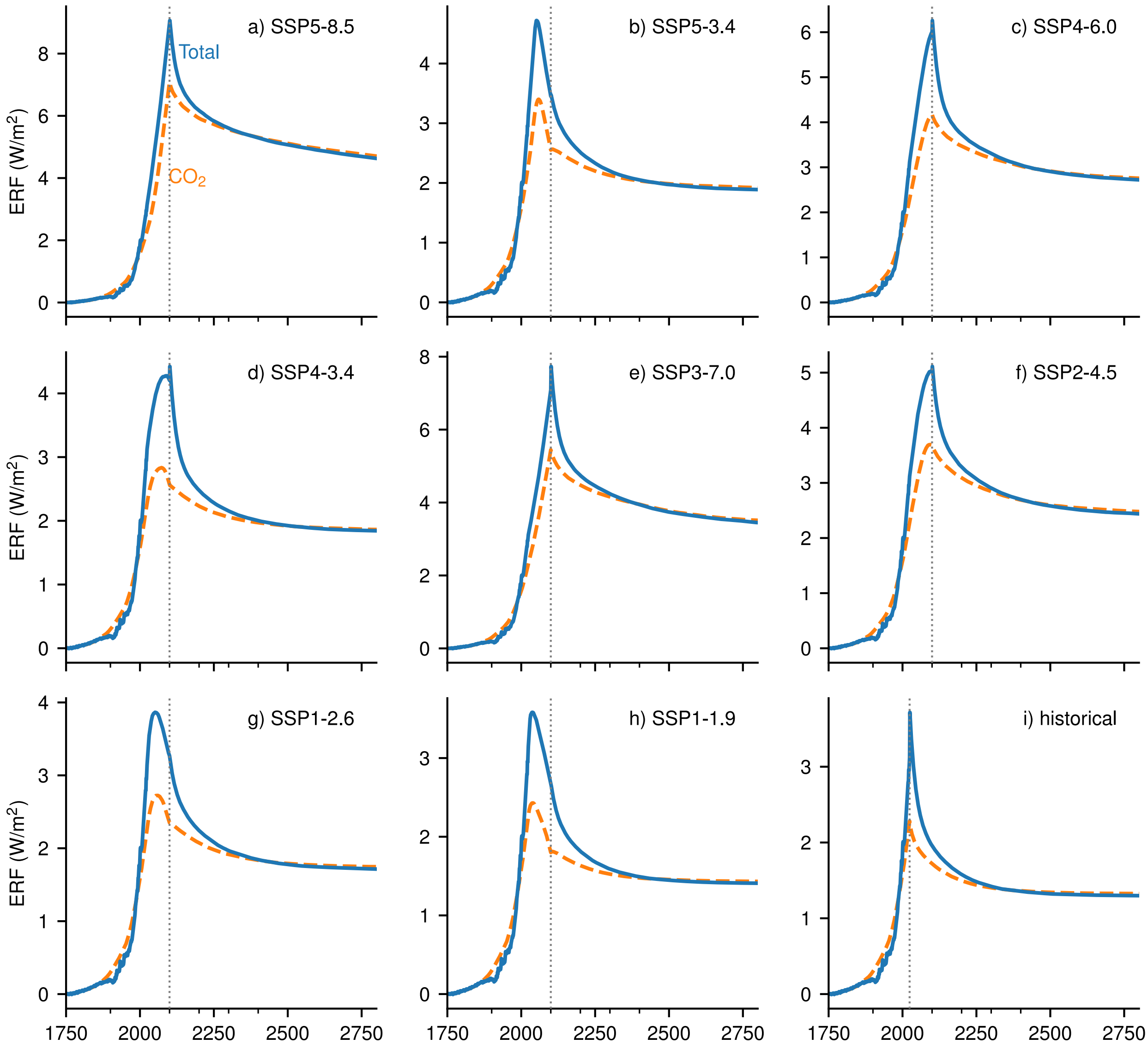

Extended Data Fig. 8 | Equilibrium forcing dominated by CO_2. The median total (blue) versus CO_2 (orange) radiative forcing simulated by the FaIR ensemble under the Shared Socioeconomic Pathways (SSPs) (panels **a**-**h**) with an immediate cessation at year 2100, alongside the historical case with cessation at 2024 (panel **i**). The cessation year is marked by a dotted vertical line in each panel.

https://doi.org/10.1038/s41558-026-02700-2

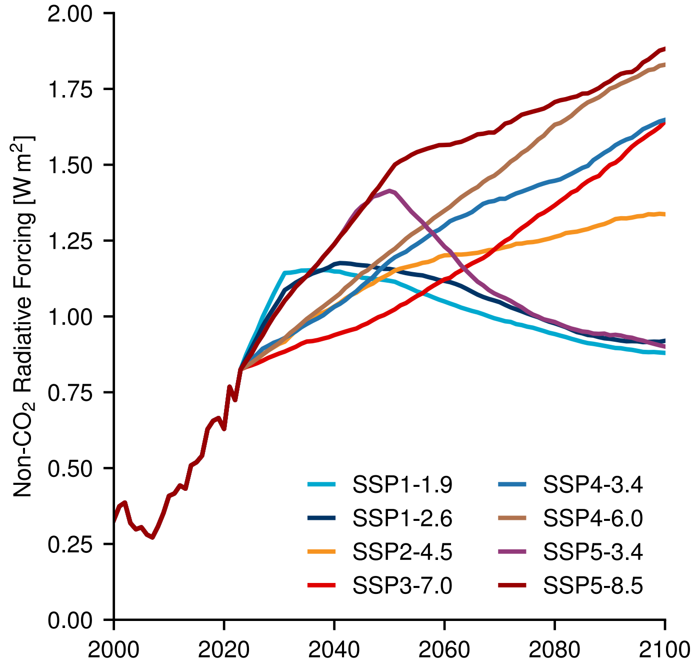

Extended Data Fig. 9 | Non-CO_2 forcing increases over the 21st century in all SSPs. The median radiative forcing not due to CO_2 as simulated by the FaIR ensemble under the Shared Socioeconomic Pathways (SSPs). Even in the mitigation SSPs, the non-CO2 radiative forcing increases from 2025 onward because declining sulfate emissions reduce the magnitude of aerosol cooling.

https://doi.org/10.1038/s41558-026-02700-2

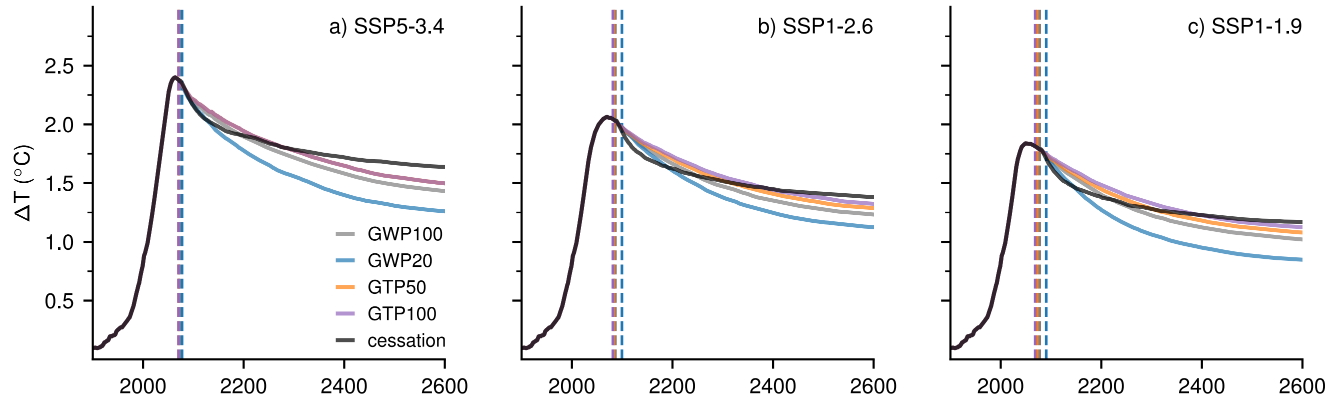

Extended Data Fig. 10 | Sensitivity to the definition of net-zero greenhouse gases. Temperature evolution in the mitigation SSPs (panels **a**-**c**) under net-zero GHG emissions. As in Fig. 4a, but with CO_2-equivalence computed using GWP20 (blue), GTP50 (orange), and GTP100 (purple), in addition to GWP100 (grey). For each metric, the year at which net-zero is reached is indicated by a dashed vertical line. After net-zero, the emissions mix is held fixed, but the magnitude of emissions declines on an exponential timescale of a century. The experiment in which emissions cease when net-zero is first achieved as defined by GWP100 is also shown (black).